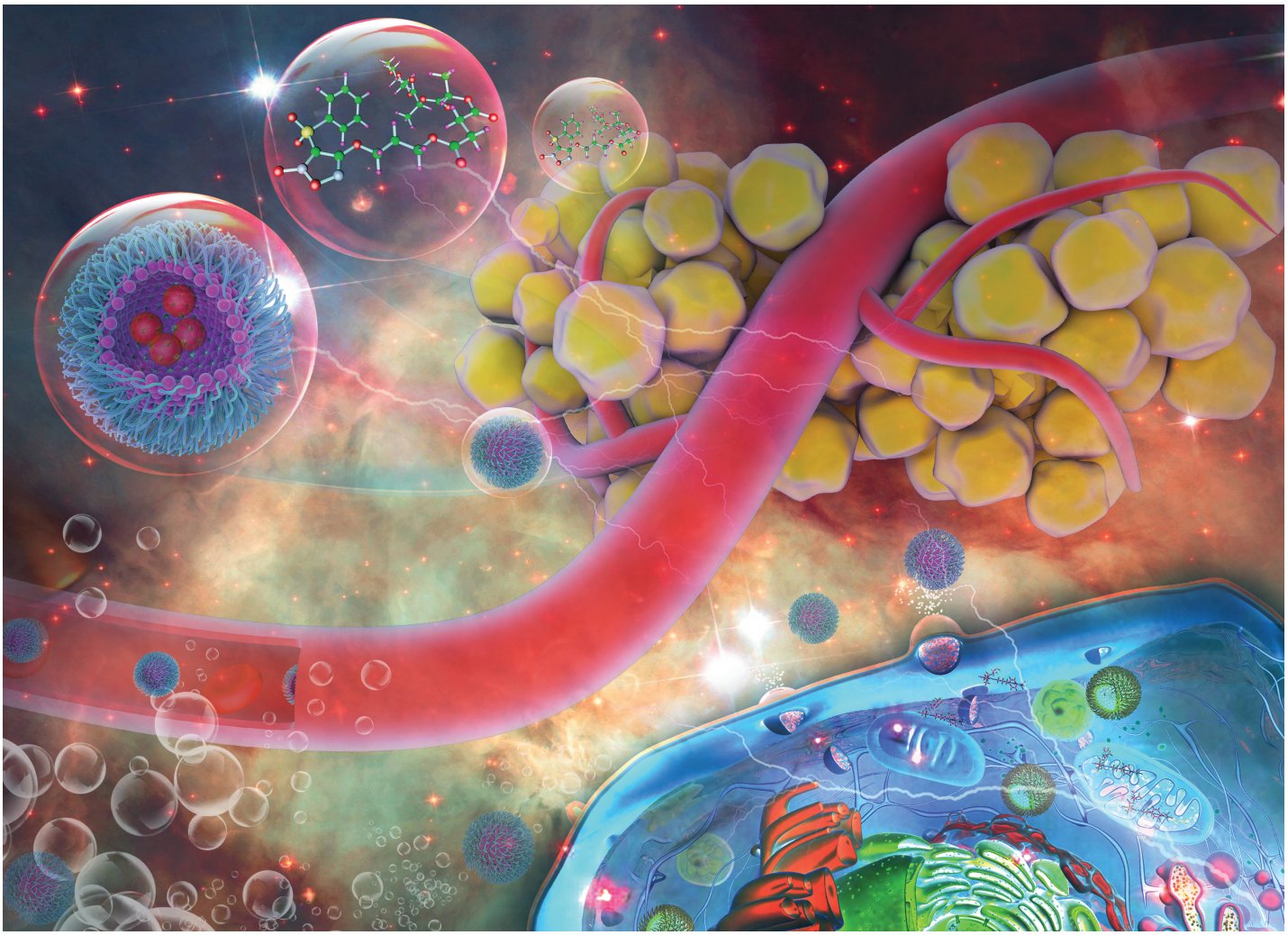

Showcasing research from the Zunhua Yang lab at the Jiangxi University of Chinese Medicine, China.

Evaluation of novel paclitaxel-loaded NO-donating polymeric micelles for an improved therapy for gastroenteric tumor

A NO-releasing polymer (mPEG-PLA-NO) is developed as micellar nanoparticle delivery system for the carrier of paclitaxel. The amphiphilic copolymer will self-assemble to form a paclitaxel-loaded micelle to release paclitaxel and NO in tumor cells and to exert improved water-solubility, enhanced antitumor effect, reduced therapeutical toxicity and anti-metastasis potential.

As featured in:

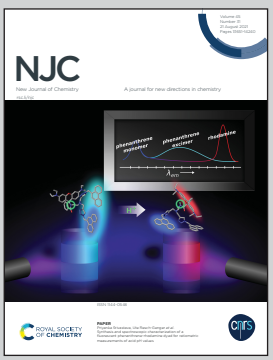

See Zunhua Yang *et al.*, *New J. Chem.*, 2021, **45**, 13763.

ROYAL SOCIETY OF CHEMISTRY

rsc.li/njc

Registered charity number: 207890

NJC

ROYAL SOCIETY OF CHEMISTRY

PAPER

View Article Online
View Journal | View Issue

Cite this: *New J. Chem.*, 2021, 45, 13763

Evaluation of novel paclitaxel-loaded NO-donating polymeric micelles for an improved therapy for gastroenteric tumor

Huilan Li,†[a] Yuanying Fang, †[b] Xiang Li,[b] Liangxing Tu,[a] Guoliang Xu,[a] Yi Jin,[b] Ronghua Liu[a] and Zunhua Yang *[a]

Received 26th February 2021,
Accepted 25th June 2021

DOI: 10.1039/d1nj00979f

rsc.li/njc

This study reports the design and synthesis of NO-donating polymer to generate biodegradable polymeric micelle containing paclitaxel (NO/PTX) as a nanomedicine delivery system aimed to enhance the solubility and anti-cancer activity of paclitaxel (PTX). NO/PTX showed greater NO-releasing performance than nitroglycerin, displaying excellent tolerance in KM mice, and exhibited a two-fold stronger antiproliferative activity than PTX *in vitro* against HCT116, SW480, and SGC-7901 cell lines. *In vivo* tumor growth inhibition assay results indicated that NO/PTX displayed lightly stronger activities against tumor growth than PTX at a dose of 10 mg kg^{-1}, while the anti-tumor effect of NO/PTX was significantly improved than that of PTX and Genexol®-PM groups at a dose of 15 mg kg^{-1} (the inhibition rate: 67% *vs.* 53% and 41%). In addition, NO/PTX showed an improved area under the plasma concentration-time curve and drug deposition in tumors in comparison to PTX. Wound healing assay and western blot analysis of EMT-related markers suggested that NO/PTX could inhibit the potential of HCT116 migration. Western blot analysis also demonstrated that NO/PTX dampened efflux activity of P-gp and up-regulated apoptosis-related proteins. Overall, these promising results suggested that the synergism between PTX and NO-donating micelles could contribute to the potent anti-cancer activity of NO/PTX.

1. Introduction

Paclitaxel (PTX) is a well-known anti-cancer drug used for treatment including breast cancer, ovarian cancer, and leukemia.[1–3] However, due to weak solubility and adverse effects, PTX has limitations and its clinical applications have to be further investigated;[4–6] aimed to increase the solubility and bioavailability of PTX, cremophor EL was added to prepare formulations as an aqueous vehicle. Unfortunately, cremophor EL is known to induce hypersensitivity and nephrotoxicity.[6,7] Thus, recently new pharmaceutical preparation techniques such as liposomes,[8,9] microspheres,[10,11] nanocapsules,[12,13] polymeric micelles[14,15] and other carriers were developed as nanomedicine delivery systems to improve the water solubility, bioavailability and lower toxicity of taxanes. Especially, polymeric micelles have attracted more attention because of their unique structure and properties.[16–18] Genexol®-PM is the first paclitaxel polymeric micelle formulation approved by South Korea, using monomethoxy poly(ethylene glycol)-polylactide (mPEG-PLA) as a carrier material,[19] The *in vivo* antitumor efficacy of Genexol®-PM against SKOV-3 human ovarian cancer and MX-1 human breast cancer is significantly greater than that of Taxol®.

Numerous studies have provided evidence that the high concentration of nitric oxide (NO) would generate a significant anti-tumor effect.[20–23] NO concentration of more than 400 nM could activate the p53 pathway, leading to cell cycle arrest and cell growth inhibition. When the concentration of NO surpassed 1 μM, the occurrence of nitrosation, nitration and alkylation would enhance the apoptosis of tumor cells by the repression of specific DNA repair systems, causing disorders of energy metabolism and disruption of mitochondrial physiology.[24,25] Furthermore, NO could improve the sensitivity of chemotherapy.[26,27] NO donors would convert the anti-apoptotic NF-κB/Snail/YY1/RKIP/PTEN resistant loop into a sensitive pro-apoptotic loop, inhibiting tumor cell viability and proliferation, and sensitize cells to apoptosis.[28,29]

NO donors could be divided structurally into several categories, including organic nitrites and nitrates, metal nitrosyls, furoxans, *S*-nitrosothiols, and diazeniumdiolates.[30] Organic nitrate-based NO donors were able to show anti-tumor activities by increasing tumor cell oxygenation capacity and tumor perfusion to inhibit tumor angiogenesis.[29] Metal nitrosyl complexes could inhibit the

[a] *College of Pharmacy, Jiangxi University of Traditional Chinese Medicine, Nanchang 330004, China. E-mail: joshyyy@126.com*
[b] *National Engineering Research Center for Manufacturing Technology of TCM Solid Preparation, Jiangxi University of Traditional Chinese Medicine, Nanchang 330006, China*

† H. L. and Y. F. contributed equally to this work.

clone formation and cell invasion of tumor cells. Furoxan was a type of thiol-based heterocyclic NO donor. Thiol first attacked position 3 or 4 of the furoxan ring, and then the ring was dearomatized and opened to release NO, which could reverse multiple drug resistance of tumor cells to make them more sensitive to chemotherapy. Diazeniumdiolates had a long half-life (20 hours at 37 °C) and could be used as long-acting NO donors. Their mechanism of action was to interact with glutathione-*S*-transferase in the human body and be catalyzed to produce NO, and then come into an antitumor effect.[31,32] NO donors could be carried by polymeric nanoparticles to increase the circulation stability and load amounts of NO in the solid tumor by the enhanced permeability and retention effect.[33–35]

Therefore, in order to improve the anti-cancer efficacy, we designed the NO donating micelle as a drug delivery system. We supposed that the synergistic effect of PTX and NO might contribute to the anti-cancer activity markedly, and nanomedicine-micelle carrier could decrease the toxicity of PTX as well. The amphiphilic copolymer is self-assembled to form a NO-donating paclitaxel-loaded micelle, which would release PTX and NO in tumor cells and exert an enhanced antitumor effect by inducing the apoptosis of tumor cells (Fig. 1).

In this work, we developed a monomethoxy poly(ethylene glycol)-polylactide (mPEG-PLA) micelles which were hybridized with furoxan-based NO donor moiety and loaded with PTX to generate a biodegradable polymeric micellar system (mPEG-PLA-NO-PTX, abbreviated as NO/PTX). We then evaluated the NO-releasing activity, acute toxicity, and antitumor efficacy *in vitro* and *in vivo*, pharmacokinetics and tissue distribution, wound healing activity, and effects on the expression of related proteins, comparing with the current clinical formulation of PTX.

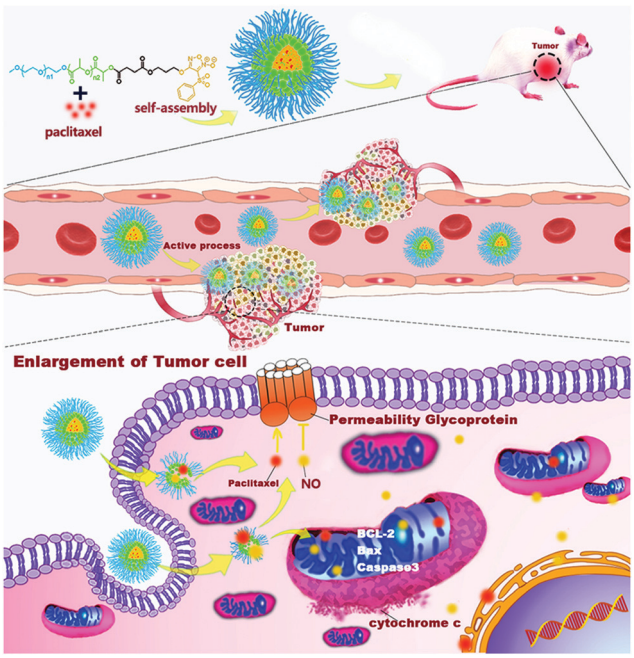

Fig. 1 Proposed mechanism of action of NO/PTX micelles.

2. Results and discussion

2.1 Synthesis and characterization of NO donating polymer

To investigate the synergistic effect of NO for cancer therapy, we developed a NO donating polymer as a nanoparticle carrier of antitumor drugs. A monomethoxy poly(ethylene glycol)-polylactide (mPEG-PLA, $M_W \approx 4$ kDa) was firstly synthesized by coupling mPEG2000 ($M_W \approx 2.2$ kDa) with DL-lactide in the presence of tin(II) octoate. The synthetic precursor furoxan was prepared through 5 steps starting from thiophenol according to the previous procedure.[36] The NO donor furoxan was treated with pivaloyl chloride to form a mixed anhydride, which was coupled with mPEG-PLA to afford the ester mPEG-PLA-NO (Scheme 1). The polymeric product was purified by fast filtration from cold ethanol and dried in a vacuum.

^{1}H NMR spectra of the polymer mPEG-PLA-NO were recorded on a 600 MHz spectrometer using deuterated chloroform ($CDCl_3$) as a solvent and tetramethylsilane (TMS) as the internal standard (Fig. 2). We could estimate the unit numbers of monomer ($n_1 + 1 \approx 49$, $n_2 + 1 \approx 27$) according to the integrals of featured peaks (δ 3.65 (m, $(4n_1 + 2)H$, –O–C$\underline{H}_2$C$\underline{H}_2$–O–), 5.14 (m, $(n_2 + 1)H$, –OCOC$\underline{H}$(CH$_3$)–O–), 1.58(m, $3(n_2 + 1)H$, –OCOCH(C$\underline{H}_3$)–O–)). The molecular weight distributions (polydispersity index, PDI = M_w/M_n) of mPEG-PLA-NO were determined to be 1.13 by gel permeation chromatography (GPC).

2.2 Preparation of PTX-loaded micelle

The polymer mPEG-PLA-NO was dissolved in ethanol with the help of surfactant HS15. PTX was also dissolved in the solution after stirring. Mannitol solution was added to form the aqueous micelle. The clear solution was lyophilized to afford the micelle of PTX (NO/PTX).

The average diameter of NO/PTX micelles, determined by dynamic light scattering (DLS), was less than 50 nm (Fig. 3A). Transmission electron microscopy (TEM, Fig. 3B) investigation showed that the micelles were spherical and had sizes consistent with that of DLS measurements. The entrapment efficiency (EE%) of PTX was determined to be 97.7 ± 0.5%.[35]

2.3 NO-releasing test

The levels of NO release abilities from PTX and NO/PTX were evaluated by the Griess method. Nitroglycerin and saline were used as positive and negative controls. As shown in Fig. 3C, while nitroglycerin released NO with a continuously growing trend within 12 hours, NO/PTX displayed a greater release performance than nitroglycerin with a peak at 6 hours. Only PTX showed almost no release of nitric oxide.

2.4 Acute toxicity

The acute toxicity for mPEG-PLA, mPEG-PLA-NO, PTX and NO/PTX were investigated in healthy male SPF KM mice. Four groups of KM mice were injected with solutions *via* the caudal vein at the dose of 1500, 2000 and 3200 mg kg^{-1} per day (mPEG-PLA or mPEG-PLA-NO) or 20, 30, 36.3, 38.84, 40.55, 42.3 and 45 mg kg^{-1} per day (PTX) or 60, 80, 120, 141.72 and 160 mg kg^{-1} per day (NO/PTX) for seven days, respectively. Saline was used

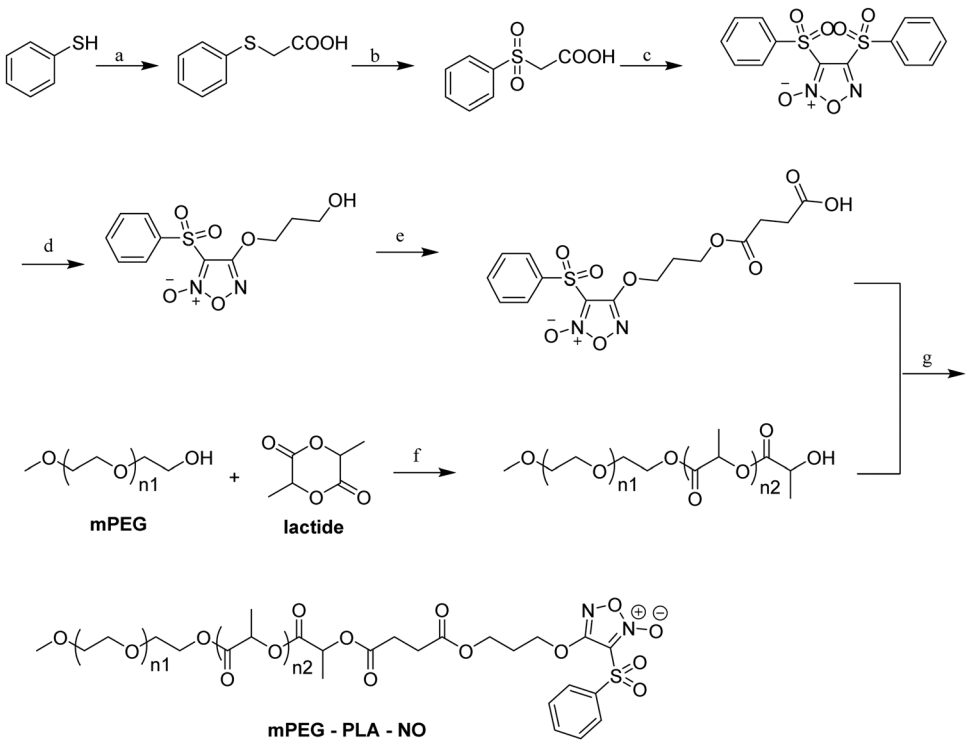

Scheme 1 Synthesis of the polymer mPEG-PLA-NO. *Reagents and conditions*: (a) $ClCH_2COOH$, NaOH, reflux, 2 h; (b) 30% H_2O_2, CH_3COOH, R.T., 2.5 h; (c) fuming HNO_3, 90 °C, 1.5 h; (d) 1,3-propanediol, 25% NaOH aq., THF, R.T., 3 h; (e) succinic anhydride, DMAP, DMF, 85 °C, 6 h; (f) tin(II) octoate, 130 °C, 18 h; (g) pivaloyl chloride, pyridine, DMAP, 0 °C to R.T., 36 h.

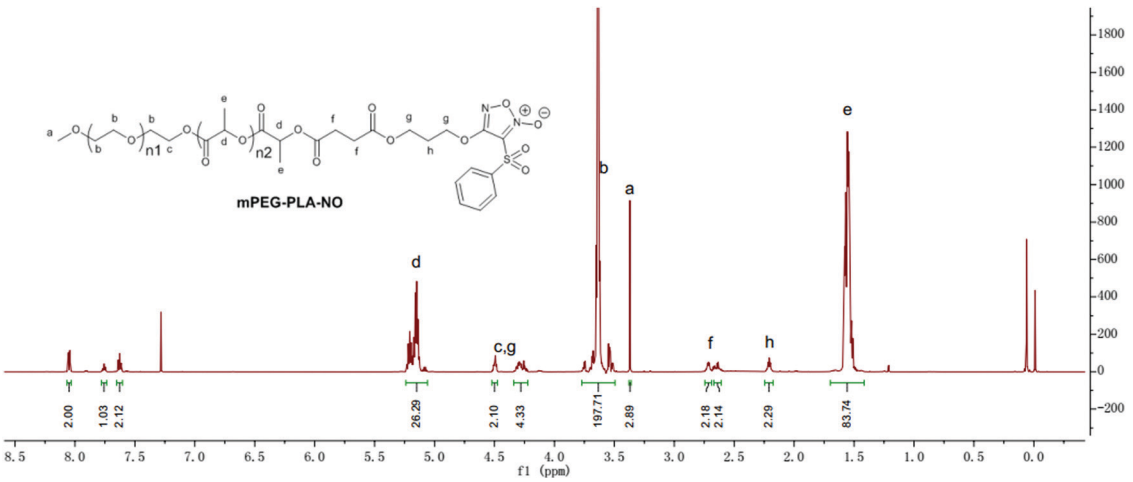

Fig. 2 ^{1}H NMR spectra of mPEG-PLA-NO in $CDCl_3$.

as a control. The median lethal dose (LD_{50}) and the maximum non-lethal dose (MNLD) were determined by Graph Pad 6. As summarized in Table 1, MNLD of mPEG-PLA and mPEG-PLA-NO were 2000 mg kg^{-1} and 1500 mg kg^{-1}, respectively, which indicated that both mPEG-PLA and mPEG-PLA-NO were non-toxic amphiphilic copolymers. LD_{50} of PTX and NO/PTX in KM mice were determined to be 39.9 mg kg^{-1} and 137.1 mg kg^{-1}, respectively. The acute toxicity of NO/PTX was reduced to 29% of PTX.

2.5 *In vitro* cytotoxicity

An MTT assay was used to evaluate the cytotoxicity of PTX and NO/PTX against human colon cancer cell lines (HCT116, SW480 and HT29), human gastric cancer cell line (SGC-7901) and human breast cancer cell line (MCF-7). The concentrations of PTX and NO/PTX were diluted 10-fold ranging from 0.0001 to 10 μg mL^{-1}. The 50% inhibitory concentration (IC_{50}) values were calculated using the software SPSS 13.0. As illustrated in Fig. 4A, NO/PTX exhibited two-fold more potent antiproliferative

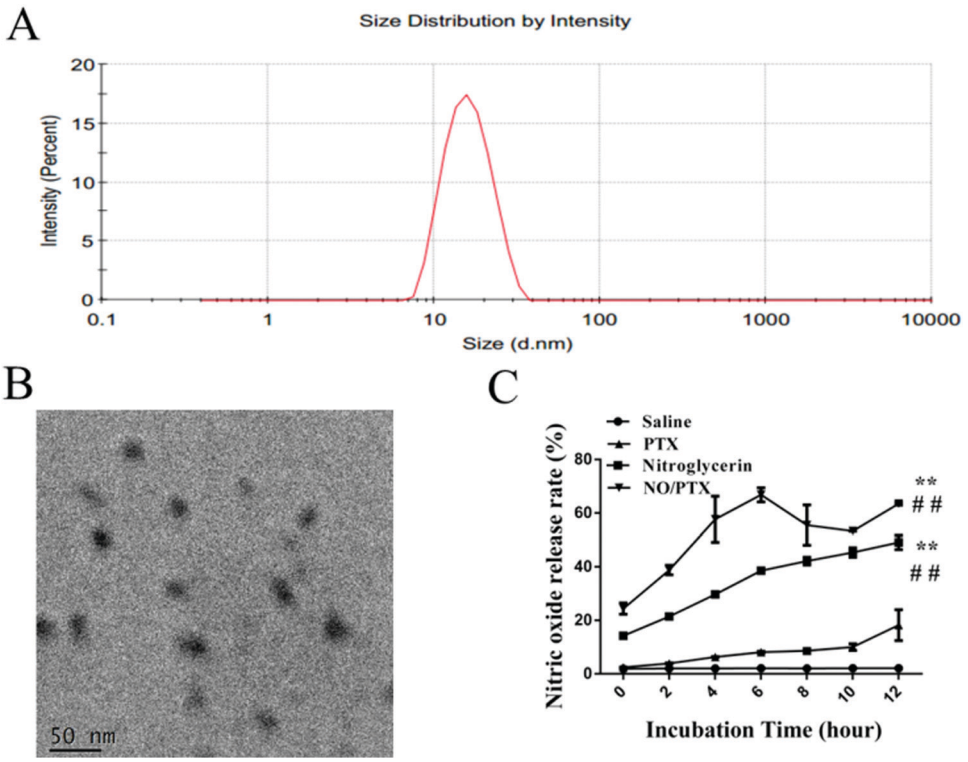

Fig. 3 The size distribution of NO/PTX micelles by DLS (A) and TEM micrograph of NO/PTX micelles (B). NO releasing ability of NO/PTX micelles (n = 3) (C). * $p < 0.05$ and ** $p < 0.01$ *vs.* saline group. #$p < 0.05$ and ##$p < 0.01$ *vs.* PTX group.

Table 1 Acute toxicities of mPEG-PLA, mPEG-PLA-NO, PTX and NO/PTX in mice

Compound	MNLD (mg kg^{-1})	LD_{50} (mg kg^{-1})
mPEG-PLA	2000	—
mPEG-PLA-NO	1500	—
PTX	36.3	39.9
NO/PTX	80	137.1

activities than PTX against HCT116, SW480 and SGC-7901, and 1.5 fold stronger activity toward MCF-7, but was less potent against HT29. These preliminary results indicated that NO/PTX displayed a more potent inhibitory effect with gastroenteric cancer than PTX.

2.6 *In vitro* wound healing assay

Since a potent antiproliferative effect was observed against the HCT116 cell line, HCT116 was selected for further studies. The inhibition of HTC116 migration by PTX and NO/PTX was assessed using a wound-healing assay. The consistent width scratched monolayer HCT116 cell line was treated with PTX or NO/PTX at concentrations of 0.01 and 0.1 μg mL^{-1}. Images in different groups were captured at 0, 12 and 24 h using a Leica DMI3008 inverted microscope. Image J software was used to calculate the wound healing area. Consequently, decreased cell motility was observed in the HTC116 cell line treated with PTX or NO/PTX (Fig. 4B). The migration potential of HTC116 cells was significantly inhibited by 0.1 μg mL^{-1} of NO/PTX at 12 and 24 h in comparison with PTX.

2.7 *In vivo* tumor growth inhibition

To investigate the *in vivo* tumor growth inhibition of our PTX-loaded NO-releasing polymeric micelle (NO/PTX), we compared its antitumor effect with commercial PTX injection and Genexol®-PM (PTX-containing mPEG-PLA polymeric micellar system). Firstly, we carried out the tumor growth inhibition assay *in vivo* using the H22 hepatocellular carcinoma model in KM mice, for H22 mice model could be conveniently available to demonstrate the efficacy and toxicity of drug clearly. After the tumors were well-established, PTX, Genexol®-PM and NO/PTX were injected *via* the caudal vein at doses of 10 and 15 mg kg^{-1} respectively on days 0, 3 and 6 with saline as the control. On day 9, mice were sacrificed and the tumor was harvested and weighted. We also tested the antitumor activity of the polymeric carriers mPEG-PLA and mPEG-PLA-NO at the dose of 300 mg kg^{-1} in the same way.

The results are shown in Fig. 5. The polymer mPEG-PLA did not show any antitumor response. A slight antitumor effect was observed in the mPEG-PLA-NO group (Fig. 5B). Significant antitumor activities were observed in PTX, Genexol®-PM and NO/PTX groups. As illustrated in Table 2, PTX, Genexol®-PM and NO/PTX groups showed comparable anti-tumor activities (inhibition rates were 39%, 36% and 41%, respectively) at a low dose (10 mg kg^{-1}). Furthermore, when the dose was up to 15 mg kg^{-1}, the anti-tumor effect of NO/PTX was significantly stronger than that of the PTX and Genexol®-PM groups (the inhibition rates of PTX, Genexol®-PM and NO/PTX group were 53%, 41% and 67%, respectively, Fig. 5A), which proved that

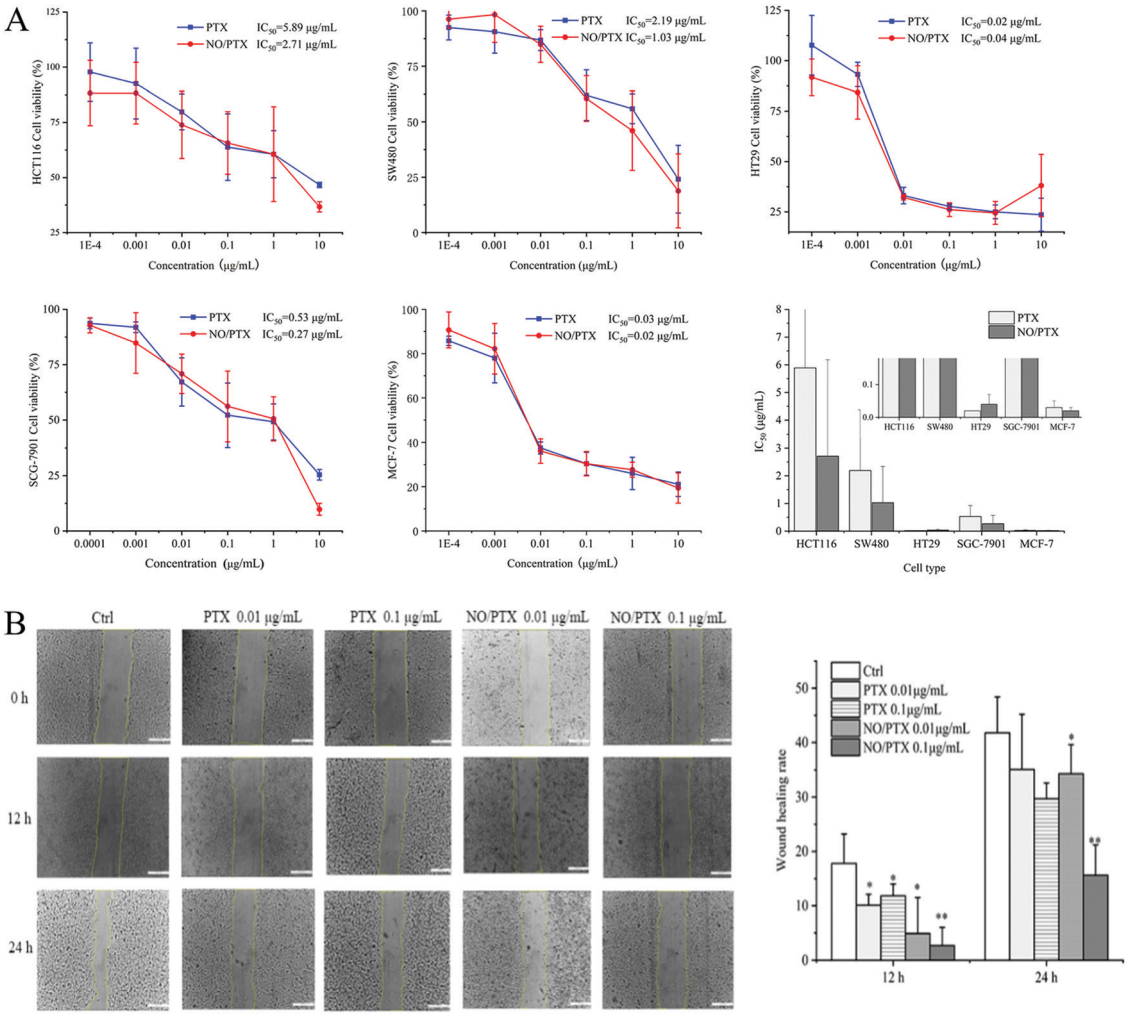

Fig. 4 Cytotoxicity of PTX and NO/PTX against HCT116, SW480, HT29, SGC-7901 and MCF-7 cell lines (A). Inhibition of HTC116 cell motility by PTX or NO/PTX (B).

the synergistic effect of NO and paclitaxel enhances the anti-tumor activity. When treated with the same dose of PTX or NO/PTX, the mice lost their similar weight, which indicated that NO/PTX did not lead to extra toxicity in contrast to PTX.

2.8 Pharmacokinetics and tissue distribution

The pharmacokinetics and tissue distribution were studied in a male KM mouse xenograft model established with H22 cells to delineate the disposition of the NO/PTX *in vivo*. According to the positive reference Genexol®-PM,[19] we also use the same dose to study the pharmacokinetics and tissue distribution. The mice were injected with PTX (20 mg kg^{-1} calculated as PTX) or NO/PTX (50 mg kg^{-1} calculated as PTX) solution in saline *via* the tail vein. Plasma and tumor were collected at 0, 0.05, 0.5, 1, 2, 3, 4, 8, 12 and 24 h. At each sampling time point, 3 to 4 mice were anesthetized with ether, and blood was collected *via* cardiac puncture from every mouse. These mice were sacrificed and all tumors were also collected. After centrifugation, about 100 μL plasma from each mouse was collected and frozen. The concentrations of PTX in plasma and in the tumor were determined by HPLC and the concentrations of PTX in the heart, liver, spleen, lungs and kidneys were determined using HPLC-MS/MS with docetaxel as internal standard. The pharmacokinetic parameters were processed by non-compartmental analysis using the DAS 2.0 software package (from the Chinese Pharmacological Society).

The pharmacokinetic parameters achieved are presented in Table 3. The levels of PTX in plasma at each time point in the NO/PTX (50 mg kg^{-1}) group were higher than PTX (20 mg kg^{-1}) group (Fig. 6A) within the first four hours because the administered dose of NO/PTX is 2.5 times higher than PTX. Then, the plasma concentrations of NO/PTX and PTX went to basically the same after 4 h. The area under the plasma concentration–time curve (AUC_{0-t}) of NO/PTX was 1.47 folds higher than that of PTX.

Paclitaxel concentrations in tumors and various tissues were illustrated in Fig. 6B and C. After i.v. administration, paclitaxel was widely distributed into most tissues. Among them, the highest paclitaxel concentration was obviously found in the tumor. The paclitaxel concentration of the NO/PTX group in the tumor was higher than the PTX group at all time points and

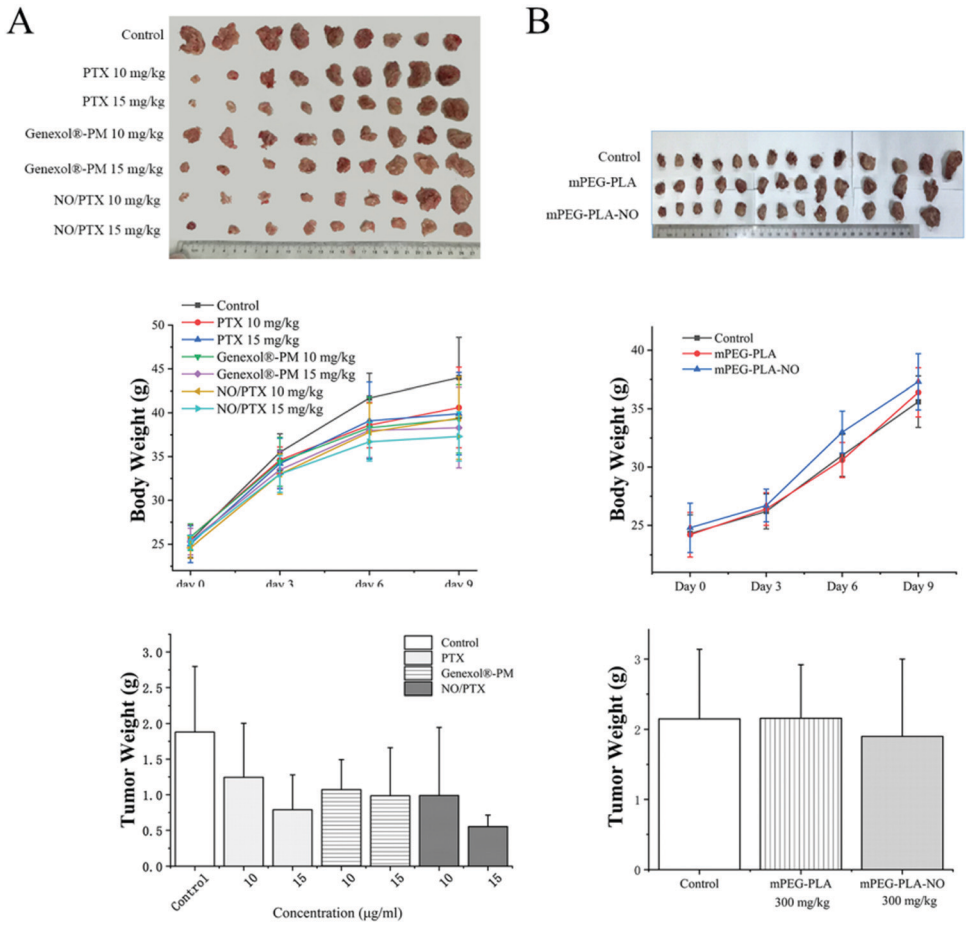

Fig. 5 Inhibition of tumor growth by (A) PTX, Genexol®-PM and NO/PTX at 10 and 15 mg kg^{-1}; by (B) mPEG-PLA and mPEG-PLA-NO.

Table 2 *In vivo* tumor growth inhibition (n = 9)

Group	Dosage mg kg^{-1}	Number of animals (n)	Body weight (g)	Tumor weight (g)	Tumor inhibition rate %
Control	—	9	34.0 ± 1.6	—	—
Saline	—	9	35.5 ± 2.1	1.67 ± 0.92	—
PTX	10	9	34.6 ± 1.5	1.03 ± 0.74	39 ± 44
PTX	15	9	34.2 ± 2.9	0.79 ± 0.49	53 ± 29
Genexol®-PM	10	9	34.4 ± 2.8	1.07 ± 0.42	36 ± 25
Genexol®-PM	15	9	33.5 ± 2.1	0.99 ± 0.68	41 ± 40
NO/PTX	10	9	33.0 ± 2.3	0.99 ± 0.96	41 ± 57
NO/PTX	15	9	33.0 ± 2.1	0.55 ± 0.16	67 ± 10

reached the maximum paclitaxel concentration in 3 h. In these organs, paclitaxel concentrations were tested at a low concentration and mostly eliminated after 24 h. Even though we observed the levels in all the tissues with NO/PTX were higher at each time point than PTX, as shown in Fig. 6C, in fact, the NO/PTX group exhibited a lower concentration of paclitaxel in these tissues at the same dose. It is indicated that NO/PTX has less accumulation in tissues and organs with improved safety.

2.9 Effects on the expression of related protein

P-Glycoprotein (P-gp) is a plasma membrane protein that acts as an efflux pump for chemotherapeutic agents, associated with

Table 3 Pharmacokinetic parameters observed in mice after i.v. PTX and NO/PTX

	Dose (mg kg^{-1})	T_{max} (h)	C_{max} (μg mL^{-1})	$t1/2\beta$ (h)	$AUC_{(0-t)}$ (μg h mL^{-1})	$AUC_{(0-\infty)}$ (μg h mL^{-1})	CL (L h^{-1} kg^{-1})	V_d (L kg^{-1})
PTX	20	0.05	71.73 ± 15.9	1.485	83.315	91.309	0.39	0.169
NO/PTX	50	0.05	105.16 ± 3.6	1.705	123.154	115.94	0.23	0.242

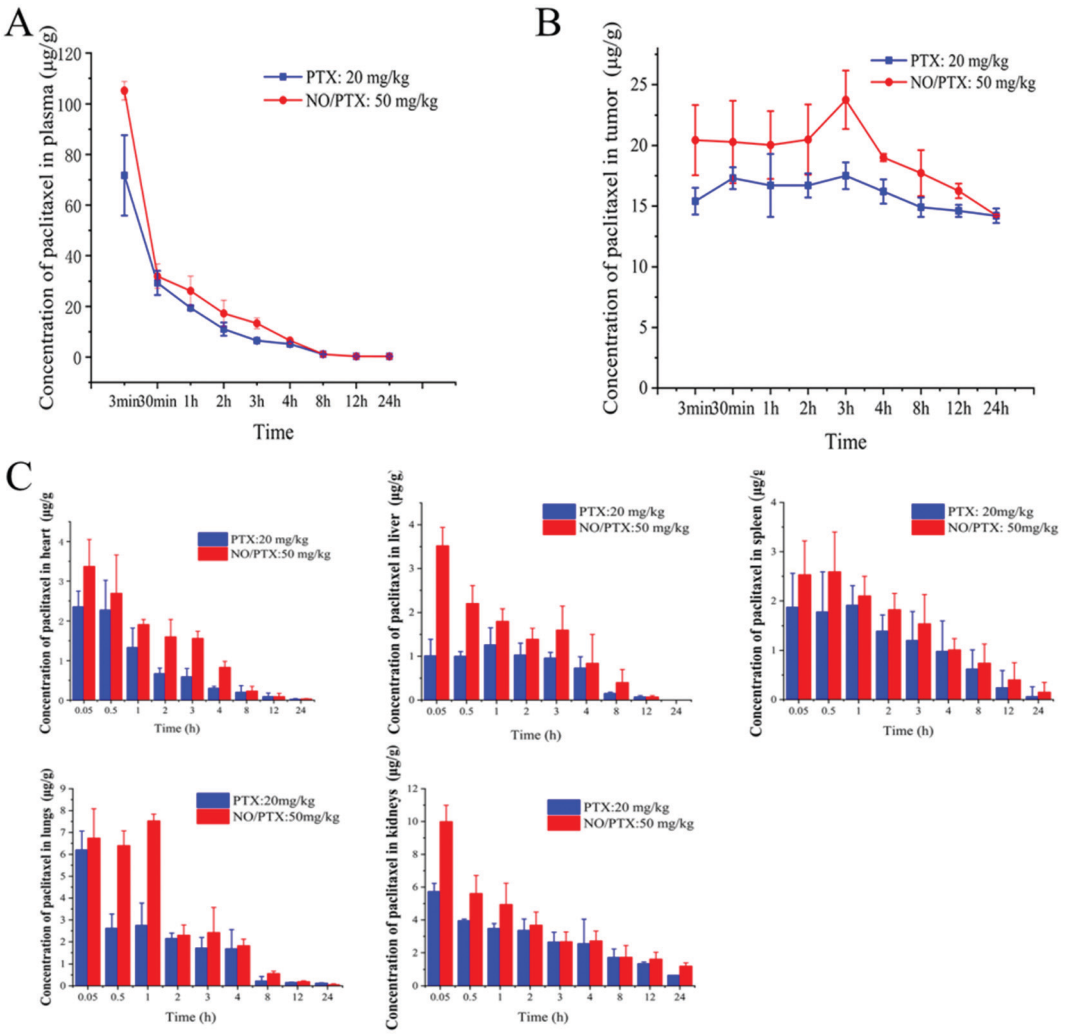

Fig. 6 Time courses of paclitaxel levels in mice plasma (A) and in mice tumor (B) and tissue distribution of paclitaxel (C) after i.v. administration of 20 mg kg^{-1} dose of PTX and 50 mg kg^{-1} dose of NO/PTX. Each point represents the mean ± S.D. of three mice per time point.

tumor multi-drug resistance.[37–39] The good antitumor effects can be achieved by inhibiting the function of P-gp or suppressing its expression. It was reported that NO donor mainly affected cellular P-gp activity by suppressing the expression of P-gp.[34,40,41] To determine whether NO/PTX was suppressing P-gp expression, we incubated HCT116, SW480, HT29, SGC-7901 and MCF-7 cells with PTX or NO/PTX and utilized western blot analysis to determine the expression level of P-gp. Compared with the control and PTX groups, NO/PTX significantly decreased P-gp expression in HCT116, SW480, HT29, SGC-7901 and MCF-7 cell lines (Fig. 7A). Using HCT116 as a high response cell line, two doses of PTX and NO/PTX were tested for suppression of P-gp. When the dose of PTX increased, the relative P-gp expression increased as well. On the contrary, the expression of P-gp was declined, in accordance with the increased amount of NO/PTX (Fig. 7B), which was consistent with the enhanced antitumor effect of NO/PTX on HCT116.

The levels of apoptosis-related proteins Bax, Bcl-2 and cleaved caspase-3 were also detected by western blot in HCT116 cell line with the treatment with PTX or NO/PTX at 0.001 or 0.01 μg mL^{-1} (Fig. 8A).[42–44] The result showed that the NO/PTX group had elevated apoptosis levels, while the control group mitigated apoptosis ($P < 0.05$). The results manifested that compared with the PTX group, the level of Cleaved-Caspase-3 and Bax in PTX and NO/PTX groups were obviously elevated, while the level of Bcl-2 was significantly decreased in the NO/PTX group.

Epithelial–mesenchymal transition (EMT) was considered to be an important mechanism for cancer cell migration and invasion.[45–47] Changes in EMT and invasive properties *in vitro* could be used to hypothesize the metastatic potential of cancer cells *in vivo*. To further investigate the inhibitory effect of NO/PTX on the migration and invasion of HCT116 cells, western blotting was used to examine the expression levels of EMT-related markers. Compared with the PTX group, the expression levels of ZO-1 protein in HCT116 cells were significantly increased, whereas the expression levels of interstitial markers vimentin were significantly reduced ($P < 0.05$; Fig. 8B).[48,49] Class III β-tubulin counteracts the

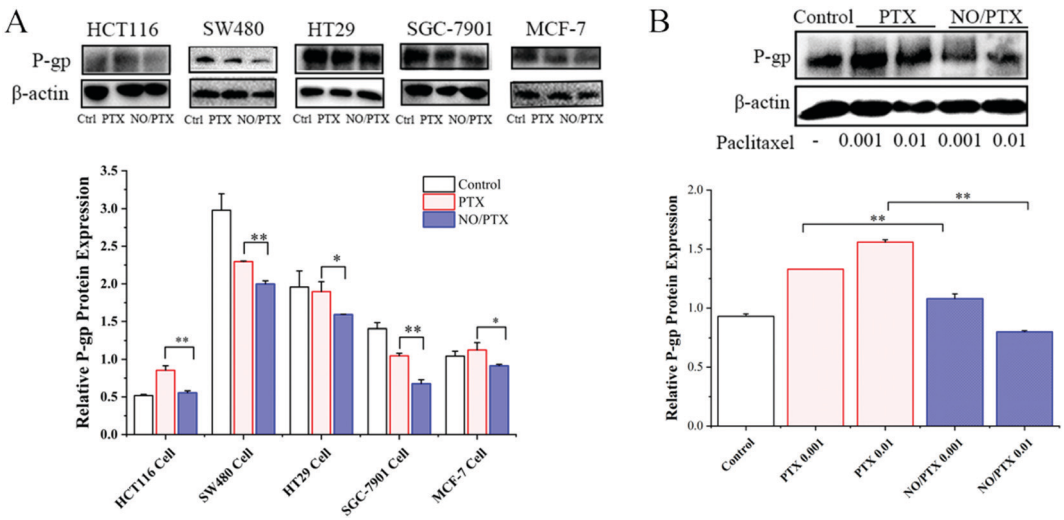

Fig. 7 NO/PTX suppressed P-gp expression in five cell lines (A). NO/PTX suppressed P-gp expression in HCT116 at 0.001 and 0.01 μg mL^{-1} (B).

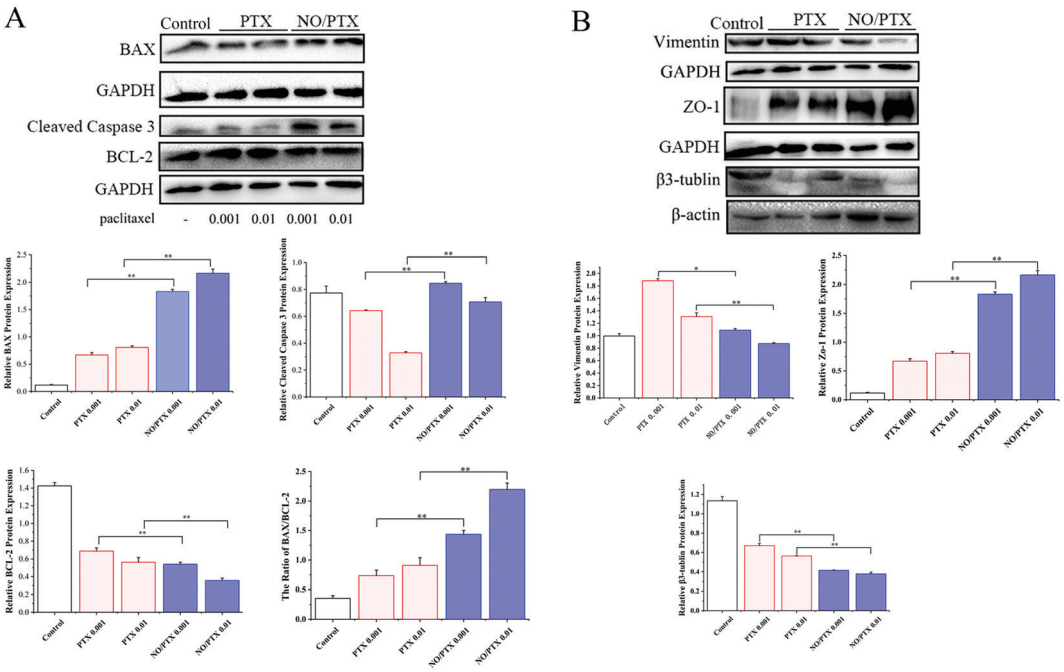

Fig. 8 NO/PTX elevated the level of Bax, Bax/Bcl-2 and cleaved caspase-3 and declined the level of Bcl-2 in HCT116 cell (A). NO/PTX elevated the level of ZO-1 and declined the level of interstitial markers vimentin and III β-tubulin in HCT116 cell (B).

ability of paclitaxel to inhibit cell migration.[50,51] Compared with the PTX group, the expression levels of Class III β-tubulin protein in the NO/PTX group were significantly reduced ($P < 0.05$). The results suggested that NO/PTX could reverse EMT in HCT116 cells.

3. Conclusion

In this study, we demonstrated that NO/PTX could release functional NO and chemotherapeutic drug paclitaxel, as a polymeric micelle-based drug delivery system for cancer therapy. We evaluated its cytotoxicity against five cancer cell lines (HCT116, SW480, HT29, SCG7901 and MCF-7). The result showed that NO/PTX was more competent in anti-proliferative activity against gastroenteric cancer cell lines such as HCT116, SW480, SGC-7901 and less competent toward HT29 than PTX at the same concentrations. *In vivo* biological activity results indicated that NO/PTX had advantages over commercially available PTX injections in terms of reduced toxicity and improvement of antitumor efficacy. Western blot analysis in HCT116 cells manifested that NO/PTX suppressed P-gp expression, elevated apoptosis-related proteins

Cleaved-Caspase-3 and Bax and decreased apoptosis-related proteins Bcl-2. NO/PTX inhibited cell migration in the wound scratch assay in HCT116 cells, and acted on epithelial–mesenchymal transition (EMT) as well to suppress the migration and invasion of cancer cells. Western blot analysis also showed NO/PTX increased levels of EMT-related markers protein ZO-1, whereas the expression levels of interstitial markers vimentin were significantly reduced. Hence, NO/PTX could be considered as a promising agent against colon cancer with the merits of lowering toxicity, enhanced solubility and antitumor activity.

4. Experimental section

4.1 Material and instruments

mPEG2000 (MW: 2220) and DL-lactide were purchased from Advanced Polymer Materials Inc. (Montreal, Canada). Paclitaxel was purchased from Sigma-Aldrich (St. Louis, MO, USA). Genexol®-PM was purchased from Samyang Biopharmaceuticals Corp. (Daejeon, South Korea). Paclitaxel injection was obtained from Sichuan Sunnyhope Pharmaceutical Co., Ltd (Chengdu, China). Chemical reagents were obtained from commercial suppliers and used without further purification. ^{1}H-NMR and ^{13}C-NMR spectra were recorded on a Bruker AVANCE III HD 600 (600 Hz) spectrometer. Chemical shifts are reported in parts per million (ppm) downfield relative to tetramethylsilane as an internal standard. HPLC Analysis was performed on a Waters Acquity® Arc™ with 2998 PDA detector. The morphology of NO/PTX nanoparticles was examined using transmission electron microscopy (TEM) (FEI, Tecnai G2 F20, USA). Its size diameter was measured using a Zetasizer Nano apparatus (ZS ZEN3690, Malvern, UK).

KM mice (4–6 weeks, 18–22 g) were provided by Hunan SJA Laboratory Animals (Hunan, China). The animal experiment was performed in accordance with China SAC/TC 281 Laboratory animal-Guideline for ethical review of animal welfare (GB/T 35892-2018) and was approved by the Experimental Animal Ethics Committee of Jiangxi University of Traditional Chinese Medicine (JZLLSC2019-0170, Nanchang, China).

4.2 Micelle preparation and characterization

To a vacuum dried mPEG2000 (30.0 g) at 130 °C in the flask was added DL-lactide (30.6 g) and tin(II) octoate (121 mg). The mixture was sealed and stirred at 130 °C for 18 h. After cooling down to room temperature, the crude product was dissolved in CH_2Cl_2 (50 mL) and cold absolute ethanol (300 mL) was added to precipitate. The solid was filtered and dried in a vacuum to afford the mPEG-PLA polymer (56.2 g).

The NO-donating furoxan derivative, synthesized according to our previous study, was coupled with mPEG-PLA polymer *via* mixed anhydride. Briefly, to the solution of furoxan compound (3.0 g) in EtOAc (30 mL) were added Et_3N (1.73 mL) and pivaloyl chloride (1.11 mL) at −10 °C. The reaction mixture was stirred at 0 °C for 2 h and filtered to remove undissolved salt. The filtrate was evaporated to give a liquid as mixed anhydride. To the solution of mPEG-PLA (12.6 g) in CH_2Cl_2 (63 mL), pyridine (1 mL) and DMAP (146 mg) were added. A solution of anhydride in CH_2Cl_2 (15 mL) was added to the mixture at 0 °C. The resulting reaction mixture was stirred at this temperature for 2 h, maintained at room temperature for 36 h, added to cold ethanol. The precipitate was collected by filtration and dried to afford the mPEG-PLA-NO polymer (12.8 g). The structure of the polymer was confirmed by ^{1}H NMR.

The polymer mPEG-PLA-NO (50 mg) and surfactant HS15 (50 mg) were dissolved in ethanol (5 mL). PTX (10 mg) was dissolved completely in the solution after stirring. Mannitol solution (5%, 1.9 mL) was added to form the aqueous micelle. The clear solution was lyophilized to afford the micellar PTX (NO/PTX).

The entrapment efficiency (EE%) of NO/PTX was determined using an ultrafiltration method by separating the non-entrapped drug from nanoparticles. EE% = $(C_{total} - C_{free})/C_{total}$.

4.3 NO-releasing test

NO was measured by the Griess reaction. Briefly, $NaNO_2$ at different concentrations was prepared for the standard curve. Nitroglycerin (0.00166 mM) and NO/PTX (0.005 mM) were incubated in an L-cysteine environment and saline was used as a control, after 1, 2, 3, 4, 6, 8, 10 h, taken 1 mL incubated solution with 1 mL Griess reagent for 10 min. The resulting absorbance values at 540 nm were determined using a microplate reader. The duration of NO release and the highest NO-release rate as essential parameters were calculated.

4.4 Acute toxicity

Acute toxicity for mPEG-PLA, mPEG-PLA-NO, PTX and NO/PTX was investigated in healthy male SPF KM mice. 5–8 mice were used per group and single i.v. doses of 1500, 2000 and 3200 mg kg^{-1} mPEG-PLA, 1500, 2000, 3000 and 3200 mg kg^{-1} mPEG-PLA-NO, 20, 30, 36.3, 38.84, 40.55, 42.3 and 45 mg kg^{-1} PTX. 60, 80, 120, 141.72 and 160 mg kg^{-1} NO/PTX, and saline as a control was injected through the tail vein. The animals were euthanatized following the animal (Control of Experiments) ordinance of laws of China, after the 7 day treatment period, and the number of mice surviving was recorded. The median lethal dose (LD_{50}) and the maximum non-lethal dose (MNLD) were determined by Graph Pad 6.

4.5 *In vitro* cytotoxicity

Human colon cancer (CRC) cell lines HCT116, SW480 and HT29, human gastric cancer cells SGC-7901, human breast cancer cell line MCF-7 were used *in vitro* cytotoxicity study. The growth-inhibitory effect of PTX and NO/PTX were assessed based on 10-fold dilutions ranging from 0.0001 up to 10 μg mL^{-1} using MTT assay. Briefly, the cells were counted and plated in 96-well plates at a density of 8×10^3 cells per well for 12 h and then treated with each drug concentration of PTX or NO/PTX in triplicate. Following 48 h of continuous drug exposure, the MTT solution (20 μL, 5.0 mg mL^{-1}) was poured into each well. After 4 h incubation, the environment containing unreacted MTT was discarded from the wells and then DMSO (150 μL) was added to each well. The OD at 570 nm was measured using a

microplate reader (Spectra MAX I3, USA). All experiments were performed independently at least three times. SPSS 13.0 software was used to analyze the 50% inhibitory concentration (IC_{50}).

4.6 *In vitro* wound-healing assay

Wound healing assays were used to evaluate the motility and metastatic potential of HTC116 cells. Briefly, cells were seeded in 6-well plates at a density of 5×10^5 cells per well, After 24 h, a 200 μL pipette tip at a consistent width was used to wound the monolayers. After scratching, the dead cells were removed and washed with PBS three times, Subsequently, PTX and NO/PTX at concentrations of 0.01 and 0.1 μg mL^{-1}, respectively, serum-free medium were added. Images in different groups were captured at 0, 12 and 24 h using a Leica DMI3008 inverted microscope. Image J software was used to calculate the wound healing area.

4.7 *In vivo* tumor growth inhibition

Mice (4–6 weeks,18–22 g) were implanted subcutaneously into the right flank with 200 μL of cell suspension containing 2×10^6 H22 cells (in PBS buffer). When the tumor had reached a volume of 50–150 mm^3 treatments were started and the day was designated on day zero. On day 0, tumor-bearing mice were randomly assigned to 7 groups with 12 mice in each group. Treated *via* the tail vein injection with 10 and 15 mg kg^{-1} PTX, 10 and 15 mg kg^{-1} Genexol®-PM, 10 and 15 mg kg^{-1} NO/PTX and saline as a control on days 0, 3 and 6. On day 9, mice were euthanized; samples of plasma and tumor were harvested and stored at −80 °C. The tumor volume was calculated, as $V = W^2 \times L/2$, where W = longer diameter and L = smaller diameter. In another separate study, 6 groups of mice were injected separately with 22.5, 45 mg kg^{-1} PTX, 22.5, 45 and 90 mg kg^{-1} NO/PTX and saline as a control. We also tested the antitumor activity of mPEG-PLA and mPEG-PLA-NO with doses of 300 mg kg^{-1} in the same way.

4.8 Pharmacokinetics and tissue distribution

The pharmacokinetics and tissue distribution were approved by the University Committee on the Use and Care of Animals, Jiangxi University of Traditional Chinese Medicines. The pharmacokinetics and tissue distribution were studied in a male KM mouse xenograft model established with H22 cells to delineate the disposition of the NO/PTX *in vivo*. The tumors were allowed to grow to about 100 mm^3. The mice were injected with PTX solution (prepared with 0.9% sodium chloride solution, 20 mg kg^{-1} calculated as PTX) or NO/PTX (50 mg kg^{-1} calculated as PTX) *via* the tail vein. Plasma and tumor were collected at 0, 0.05, 0.5, 1, 2, 3, 4, 8, 12 and 24 h. At each sampling time point, 3 to 4 mice were anesthetized with ether, and blood was collected *via* cardiac puncture from every mouse. Then, these mice were sacrificed, and all tumors were also collected. After centrifugation, about 100 μL plasma from each mouse was collected and frozen. The concentration of PTX in plasma and tumor was determined by HPLC. The concentration of PTX in the heart, liver, spleen, lungs and kidneys was determined using HPLC-MS/MS.

The pharmacokinetic parameters were processed by non-compartmental analysis using the DAS 2.0 software package (Chinese Pharmacological Society). The plasma or tumor concentration at different times was expressed as mean ± standard deviation (S.D.), and the mean concentration–time curves were plotted. The maximum plasma or tumor concentration (C_{max}) and the time to reach it was observed directly from the concentration–time curves. The area under the plasma concentration–time curve from zero to the time of the final measurable sample (AUC_{0-t}) was calculated using the linear-trapezoidal rule up to the last sampling point with the detectable level (C).

Plasma and tumor samples were pretreated with the liquid–liquid extraction method as the plasma, and the ethyl acetate–dichloromethane–acetonitrile (4 : 1 : 1) was the extraction solvent. HPLC for the analysis of PTX and docetaxel (internal standard) in plasma and tumor was performed on a Waters ACQuity Arc system (Milford, MA, USA) with the Empower 3 software (Waters) and a PDA detector (2998, Waters). The analytes were separated on a hyersil ODS2 column (4.6 × 250 mm, 5.0 μm; Guangzhou, China) with a wavelength of 227 nm. The analytes were eluted by acetonitrile: water (40 : 60, v/v, plasma) and (42 : 58, v/v, tumor).

The samples from the heart, liver, spleen, lungs and kidneys were also pre-treated by liquid–liquid extraction with ethyl acetate–dichloromethane–acetonitrile (4 : 1 : 1) as the extraction solvent.

A Shimadzu LC-VP HPLC system (Kyoto, Japan) consisting of an LC-30AD pump and a SIL-30AC autosampler was used for the separation of PTX and docetaxel on a Welch Ultimate UHPLC AQ-C18 column (100 × 2.1 mm, 1.7 μm; Shanghai, China). The mobile phase was a mixture of 0.1% formic acid in water (v/v) (mobile phase A) and acetonitrile (mobile phase B). The gradient elution program was as followed: 55% B, 0 min; 55–80% B, 0–3.0 min; 55% B, 3.1–5.0 min.

MS analysis was performed on a Triple Quad 4500 system from Applied Biosystems (MDS-Sciex, Concord, Canada) equipped with Turbo V sources and Turbo Ionspray™ interface. The electrospray ionization (ESI) source was used in a positive mode, and the mass spectrometric parameters were optimized as followed: turbo ion spray temperature, 500 °C; ion spray voltage, 5500 V; curtain gas, nitrogen, 35 L min^{-1}; nebulizing gas, 40 L min^{-1}; turbo ion spray gas, 40 L min^{-1}; entrance potential, 10 V; collision cell exit potential, 14 V. The declustering potentials for PTX and docetaxel were adjusted to 108 and 95 V, respectively. The optimized collision energies for PTX and docetaxel were 20 and 10 eV, respectively. Quantification was performed using multiple reactions monitoring (MRM) and the optimized MRM transitions were 854.3 → 286.1 for PTX and 808.6 → 226.3 for docetaxel. The quadrupoles Q1 and Q3 were set on the unit resolution. Analyst Software™ (version 1.6.2) was used to process the obtained data.

All methods were validated according to the Guidance for Industry, Bioanalytical, Method Validation (US Food and Drug Administration).

The statistical differences were tested using a one-tailed Student *t*-test at the $p < 0.01$ or at the $p < 0.05$ level.

4.9 Effects on the expression of related protein

Total proteins were extracted from HCT116 cells after treatment, followed by the determination of protein concentration using the BCA Protein Assay Kit (ComWin Biotech Co., Ltd, Beijing, China).

Equal amounts of protein (35 μg) were subjected to 7.5% or 12.5% SDS-PAGE and transferred to the PVDF membrane. After blocking with 5% nonfat milk for 2 h at room temperature, the membranes were then incubated with primary antibodies against P-gp, anti-BCL-2, anti-BAX, anti-cleaved caspase 3, anti-vimentin, anti-ZO-1, anti-Class III β-Tubulin, anti-β-actin, anti-GAPDH with gentle rotation overnight at 4 °C. Following incubation with secondary antibody conjugated with horseradish peroxidase (HRP) for 1 h at room temperature, the immunoreactive bands were visualized by the enhanced chemiluminescent (ECL) reagent (ComWin Biotech Co., Ltd., Beijing, China).

Author contributions

Huilan Li: data curation, formal analysis, investigation, writing – original draft. Yuanying Fang: conceptualization, data curation, writing – review & editing, funding acquisition. Xiang Li: methodology, investigation. Liangxing Tu: formal analysis. Guoliang Xu: project administration. Yi Jin: conceptualization, writing – review & editing, Ronghua Liu: investigation. Zunhua Yang: conceptualization, formal analysis, funding acquisition, writing – review & editing.

Conflicts of interest

The authors declare no conflicts of interest.

Acknowledgements

This study was supported by Jiangxi Provincial Department of Science and Technology (20192ACB21012), the Education Department of Jiangxi Province on Science and Technology Project Foundation (GJJ201211), Jiangxi University of Traditional Chinese Medicine (JXSYLXK-ZHYAO013) and Nanchang Innovative Talent Team (No. [2018]274).

References

1 T. S. Mok, Y. L. Wu, S. Thongprasert, C. H. Yang, D. T. Chu, N. Saijo, P. Sunpaweravong, B. Han, B. Margono, Y. Ichinose, Y. Nishiwaki, Y. Ohe, J. J. Yang, B. Chewaskulyong, H. Jiang, E. L. Duffield, C. L. Watkins, A. A. Armour and M. Fukuoka, *N. Engl. J. Med.*, 2009, **36110**, 947.
2 L. Wang, X. Zhao, F. Yang, W. Wu, M. Wu, Y. Li and X. Zhang, *Int. J. Biol. Macromol.*, 2019, **138**, 207.
3 U. Gupta, S. Sharma, I. Khan, A. Gothwal, A. K. Sharma, Y. Singh, M. K. Chourasia and V. Kumar, *Int. J. Biol. Macromol.*, 2017, **98**, 810.
4 R. T. Liggins, W. L. Hunter and H. M. Burt, *J. Pharm. Sci.*, 1997, **8612**, 1458.
5 M. Markman, A. Kennedy, K. Webster, B. Kulp, G. Peterson and J. Belinson, *J. Clin. Oncol.*, 2000, **181**, 102.
6 R. B. Weiss, R. C. Donehower, P. H. Wiernik, T. Ohnuma, R. J. Gralla, D. L. Trump, J. R. Baker, D. A. Van Echo, D. D. Von Hoff and B. Leyland-Jones, *J. Clin. Oncol.*, 1990, **87**, 1263.
7 C. Luo, Y. Wang, Q. Chen, X. Han, X. Liu, J. Sun and Z. He, *Mini-Rev. Med. Chem.*, 2012, **12**, 434.
8 X. Li, C. Fan, Z. Xiao, X. Li, C. Fan, Z. Xiao, Y. Zhao, H. Zhang, J. Sun, Y. Zhuang, X. Wu, J. Shi and Y. Chen, J. Dai, *Biomaterials*, 2018, **183**, 114.
9 J. Xue, Z. Zhao, L. Zhang, L. Xue, S. Shen, Y. Wen, Z. Wei, L. Wang, L. Kong, H. Sun, Q. Ping, R. Mo and C. Zhang, *Nat. Nanotechnol.*, 2017, **127**, 692.
10 J. You, R. Shao, X. Wei, S. Gupta and C. Li, *Small*, 2010, **69**, 1022.
11 Y. Yang, Z. Huang, J. Li, Z. Mo, Y. Huang, C. Ma, W. Wang, X. Pan and C. Wu, *Adv. Healthcare Mater.*, 2019, **8**, 1900965.
12 M. M. Hasani-Sadrabadi, V. Karimkhani, F. S. Majedi, J. J. Van Dersarl, E. Dashtimoghadam, F. Afshar-Taromi, H. Mirzadeh, A. Bertsch, K. I. Jacob, P. Renaud, F. J. Stadler and I. Kim, *Adv. Mater.*, 2014, **2619**, 3118.
13 Y. Dai, C. Xu, X. Sun and X. Chen, *Chem. Soc. Rev.*, 2017, **4612**, 3830.
14 J. R. Upponi, K. Jerajani, D. K. Nagesha, P. Kulkarni, S. Sridhar, C. Ferris and V. P. Torchilin, *Biomaterials*, 2018, **170**, 26.
15 T. Chen, L. Tu, G. Wang, N. Qi, W. Wu, W. Zhang and J. Feng, *Int. J. Pharm.*, 2020, **578**, 119105.
16 K. Luo, S. Yin, R. Zhang, H. Yu, G. Wang and J. Li, *Int. J. Pharm.*, 2020, **589**, 119870.
17 K. Hadinoto, A. Sundaresan and W. S. Cheow, *Eur. J. Pharm. Biopharm.*, 2013, **85**, 427.
18 K. Y. Choi, K. H. Min, H. Y. Yoon, K. Kim, J. H. Park, I. C. Kwon, K. Choi and S. Y. Jeong, *Biomaterials*, 2011, **32**, 1880.
19 S. C. Kim, D. W. Kim, Y. H. Shim, J. S. Bang, H. S. Oh, S. Wan Kim and M. H. Seo, *J. Controlled Release*, 2001, **72**, 191.
20 M. Studenovsky, L. Sivak, O. Sedlacek, R. Konefal, V. Horkova, T. Etrych, M. Kovar, B. Rihova and M. Sirova, *J. Controlled Release*, 2018, **269**, 214.
21 P. N. Coneski and M. H. Schoenfisch, *Chem. Soc. Rev.*, 2012, **4110**, 3753.
22 B. Bonavida and H. Garban, *Redox Biol.*, 2015, **6**, 486.
23 S. Waheed, R. Cheng, Y. Casablanca, G. Maxwell, D. Wink and V. Syed, *Molecules*, 2019, **24**, 3722.
24 V. Somasundaram, D. Basudhar, G. Bharadwaj, J. H. No, L. A. Ridnour, R. Y. S. Cheng, M. Fujita, D. D. Thomas, S. K. Anderson, D. W. McVicar and D. A. Wink, *Antioxid. Redox Signaling*, 2019, **308**, 1124.
25 W. Xu, L. Liu, I. Charles and S. Moncada, *Nat. Cell Biol.*, 2004, **611**, 1129.
26 J. Kim, B. Yung, W. J. Kim and X. Chen, *J. Controlled Release*, 2017, **263**, 223.
27 Y. C. Sung, P. R. Jin, L. A. Chu, F. F. Hsu, M. R. Wang, C. C. Chang, S. J. Chiou, J. T. Qiu, D. Y. Gao, C. C. Lin, Y. S. Chen, Y. C. Hsu, J. Wang, F. N. Wang, P. L. Yu, A. S. Chiang, A. Y. Wu, J. J. Ko, C. P. Lai, T. T. Lu and Y. Chen, *Nat. Nanotechnol.*, 2019, **1412**, 1160.
28 B. Bonavida, *Redox Biol.*, 2015, **5**, 415.
29 H. Yasuda., *Nitric oxide*, 2008, **192**, 205.

30 A. W. Carpenter and M. H. Schoenfisch, *Chem. Soc. Rev.*, 2012, **4110**, 3742.
31 V. Ciccone, M. Monti, E. Monzani, L. Casella and L. Morbidelli, *Oncotarget*, 2018, **917**, 13353.
32 Q. Li, P. Zou, J. Sun and L. Chen, *Eur. J. Med. Chem.*, 2018, **143**, 732.
33 S. Kudo and Y. Nagasaki, *J. Controlled Release*, 2015, **217**, 256.
34 M. F. Chung, H. Y. Liu, K. J. Lin, W. T. Chia and H. W. Sung, *Angew. Chem., Int. Ed.*, 2015, **5434**, 9890.
35 S. Sindhwani, A. M. Syed, J. Ngai, B. R. Kingston, L. Maiorino, J. Rothschild, P. MacMillan, Y. Zhang, N. U. Rajesh, T. Hoang, J. L. Y. Wu, S. Wilhelm, A. Zilman, S. Gadde, A. Sulaiman, B. Ouyang, Z. Lin, L. Wang, M. Egeblad and W. C. W. Chan, *Nat. Mater.*, 2020, **195**, 566.
36 Y. Fang, R. Wang, M. He, H. Huang, Q. Wang, Z. Yang, Y. Li, S. Yang and Y. Jin, *Bioorg. Med. Chem. Lett.*, 2017, **27**, 98.
37 R. W. Robey, K. M. Pluchino, M. D. Hall, A. T. Fojo, S. E. Bates and M. M. Gottesman, *Nat. Rev. Cancer*, 2018, **18**, 452.
38 S. Dallavalle, V. Dobričić, L. Lazzarato, E. Gazzano, M. Machuqueiro, I. Pajeva, I. Tsakovska, N. Zidar and R. Fruttero, *Drug Resist. Updates*, 2020, **50**, 100682.
39 A. M. Pasello, A. M. Giudice and K. Scotlandi, *Semin. Cancer Biol.*, 2020, **60**, 57.
40 H. Zhang, H. Xu, C. Ashby, Y. Assaraf, Z. Chen and H. M. Liu, *Med. Res. Rev.*, 2021, **41**, 525.
41 B. K. Sinha, C. D. Bortner, R. P. Mason and R. E. Cannon, *Biochim. Biophys. Acta, Gen. Subj.*, 2018, **186212**, 2806.
42 R. Singh, A. Letai and K. Sarosiek, *Nat. Rev. Mol. Cell Biol.*, 2019, **20**, 175.
43 J. A. Keeble and A. P. Gilmore, *Cell Res.*, 2007, **1712**, 97.
44 N. Van Opdenbosch and M. Lamkanfi, *Immunity*, 2019, **506**, 1352.
45 M. A. Nieto, R. Y. Huang, R. A. Jackson and J. P. Thiery, *Cell*, 2016, **1661**, 21.
46 O. D. Persa and C. M. Niessen, *Nat. Cell Biol.*, 2019, **213**, 299.
47 J. Yang, P. Antin, G. Berx, C. Blanpain, T. Brabletz, M. Bronner, K. Campbell, A. Cano, J. Casanova, G. Christofori, S. Dedhar, R. Derynck, H. L. Ford, J. Fuxe, A. García de Herreros, G. J. Goodall, A. K. Hadjantonakis, R. J. Y. Huang, C. Kalcheim, R. Kalluri, Y. Kang, Y. Khew-Goodall, H. Levine, J. Liu, G. D. Longmore, S. A. Mani, J. Massagué, R. Mayor, D. McClay, K. E. Mostov, D. F. Newgreen, M. A. Nieto, A. Puisieux, R. Runyan, P. Savagner, B. Stanger, M. P. Stemmler, Y. Takahashi, M. Takeichi, E. Theveneau, J. P. Thiery, E. W. Thompson, R. A. Weinberg, E. D. Williams, J. Xing, B. P. Zhou and G. Sheng, EMT International Association (TEMTIA), *Nat. Rev. Mol. Cell Biol.*, 2020, **216**, 341.
48 W. Saentaweesuk, N. Araki, K. Vaeteewoottacharn, A. Silsirivanit, W. Seubwai, C. Talabnin, K. Muisuk, B. Sripa, S. Wongkham, S. Okada and C. Wongkham, *Oncol. Res.*, 2018, **264**, 605.
49 A. E. Patteson, K. Pogoda, F. J. Byfield, K. Mandal, Z. Ostrowska-Podhorodecka, E. E. Charrier, P. A. Galie, P. Deptuła, R. Bucki, C. A. McCulloch and P. A. Janmey, *Small*, 2019, **15**, e1903180.
50 A. Ganguly, H. Yang and F. Cabral, *Oncotarget*, 2011, **25**, 368.
51 K. Sobierajska, K. Wieczorek, W. M. Ciszewski, I. Sacewicz-Hofman, M. E. Wawro, M. Wiktorska, J. Boncela, I. Papiewska-Pajak, P. Kwasniak, E. Wyroba, C. S. Cierniewski and J. Niewiarowska, *Biochim. Biophys. Acta*, 2016, **18639**, 2221.

